

---

# PG-LRF: Physiology-Guided Latent Rectified Flow for Electro-Hemodynamic PPG-to-ECG Generation

---

Xiaoda Wang<sup>1,3</sup>, Minxiao Wang<sup>2</sup>, Kaiqiao Han<sup>3</sup>, Defu Cao<sup>4</sup>, Ching Chang<sup>3</sup>, Yidan Shi<sup>3</sup>,  
Runze Yan<sup>2</sup>, Xiao Luo<sup>5</sup>, Yan Liu<sup>4</sup>, Xiao Hu<sup>2</sup>, Yizhou Sun<sup>3</sup>, Wei Wang<sup>3</sup>, Carl Yang<sup>1</sup>

<sup>1</sup>Department of Computer Science, Emory University

<sup>2</sup>Nell Hodgson Woodruff School of Nursing, Emory University

<sup>3</sup>Department of Computer Science, University of California, Los Angeles

<sup>4</sup>Department of Computer Science, University of Southern California

<sup>5</sup>Department of Statistics, University of Wisconsin–Madison

## Abstract

Electrocardiography (ECG) is the clinical standard for cardiac assessment but requires dedicated hardware that does not scale to daily-life monitoring. Photoplethysmography (PPG) is ubiquitous in wearables but lacks ECG-specific diagnostic morphology and is corrupted by motion and sensor noise. PPG-to-ECG generation aims to bridge this gap by recovering electrical morphology and timing from peripheral pulse signals. However, existing methods largely rely on statistical alignment and data-driven generation. They fail to explicitly structure the latent space around physiology-aware electro-hemodynamic factors and lack constraints from forward physiological dynamics. To address these challenges, we propose **PG-LRF**, a physiology-guided latent rectified flow framework. PG-LRF introduces an electro-hemodynamic simulator that co-models ECG and PPG through shared cardiac phase dynamics. Guided by this simulator, a Physiology-Aware AutoEncoder learns a structured electro-hemodynamic latent space. Then we integrate this simulator guidance into a PPG-conditioned latent rectified flow, enforcing ECG-side morphology consistency and ECG-to-PPG forward hemodynamic consistency during generative transport. Experiments on the large-scale MC-MED dataset demonstrate that PG-LRF significantly improves PPG-to-ECG generation and downstream cardiovascular disease classification, proving its ability to generate ECGs that are both signal-faithful and physiologically plausible under the ECG-to-PPG hemodynamic pathway.

## 1 Introduction

Electrocardiography (ECG) is the clinical standard for measuring cardiac electrical activity and diagnosing cardiovascular conditions [14, 32, 2]. However, continuous ECG monitoring requires dedicated electrodes and stable skin contact, limiting its scalability in daily-life settings. Photoplethysmography (PPG), in contrast, is widely available in consumer wearables, offering a low-cost measurement of peripheral blood-volume changes [1, 4]. Despite its appeal, PPG is fundamentally limited by high levels of motion artifacts and the inherent absence of diagnostic electrical features like P-QRS-T morphology [11, 3]. As a delayed hemodynamic response, raw PPG is structurally deficient for direct and reliable clinical diagnosis. Overcoming this bottleneck by generating diagnostically informative ECGs from wearable PPG therefore provides a highly meaningful bridge between ubiquitous sensing and verifiable cardiac assessment [27, 31, 28].

Recent PPG-to-ECG studies have progressed from supervised waveform reconstruction to adversarial and latent diffusion-based generation [31, 28, 7, 10]. Despite these advances, most existing methods

treat PPG-to-ECG generation primarily as a data-driven cross-modal translation problem, leaving two key challenges: (i) *Lack of physiology-aware latent abstraction*. PPG and ECG are coupled but asymmetric observations of the same cardiovascular process: ECG reflects upstream electrical activation, whereas PPG captures the delayed peripheral pulse. Purely statistical alignment fails to explicitly encode this directional physiological coupling. (ii) *Missing physiological simulator guidance*. Existing methods optimize data-driven signal similarity and easily hallucinate physically impossible hemodynamic delays, ignoring cardiac-cycle dynamics and the forward ECG-to-PPG hemodynamic pathway [31, 24]. Incorporating this knowledge is non-trivial; naively imposing a fixed simulator as a hard constraint risks severe model mismatch and over-regularization. A robust approach must instead integrate simulator knowledge as soft, phase-aware guidance while retaining the flexibility of data-driven latent generation.

To address these challenges, we propose PG-LRF, a physiology-guided latent rectified flow framework for electro-hemodynamic PPG-to-ECG generation. We introduce a novel electro-hemodynamic simulator that explicitly co-models ECG and PPG by linking an upstream electrical readout with a delayed peripheral pulse via shared cardiac phase dynamics. Using this simulator as a physiological anchor, PG-LRF employs a Physiology-Aware AutoEncoder (PAE) to abstract modality-specific observations into a structured cardiovascular latent space regularized by cross-modal alignment and latency-aware consistency. On top of this latent space, PG-LRF introduces a simulator-guided latent rectified flow. During training, the generative transport is explicitly regularized by the simulator to ensure both ECG-side morphological fidelity and forward ECG-to-PPG hemodynamic consistency. In summary, our main contributions are as follows:

- ❶ **Physiology-Guided Generative Formulation.** We introduce PG-LRF, formulating PPG-to-ECG generation as an electro-hemodynamic generation problem. We design an electro-hemodynamic physiological simulator to co-model ECG and PPG through shared cardiac phase dynamics, upstream electrical readouts, and delayed hemodynamic readouts.
- ❷ **Physiology-Aware Representation Learning.** We design a Physiology-Aware AutoEncoder that abstracts modality-specific observations into a structured electro-hemodynamic latent space, rigorously constrained by simulator-derived latency-aware consistency, and cross-modal latent alignment.
- ❸ **Simulator-Guided Flow Matching.** We integrate the electro-hemodynamic simulator into PPG-conditioned latent rectified flow. Simulator-derived constraints guide the model to generate ECGs that are waveform-faithful and physiologically plausible under the ECG-to-PPG hemodynamic pathway.
- ❹ **Multi-Level Experimental Validation.** We demonstrate that PG-LRF consistently improves PPG-to-ECG generation across waveform fidelity, clinical interval consistency, and cardiovascular disease detection on the large-scale MC-MED dataset.

## 2 Related Work

**PPG-to-ECG Generation.** PPG-to-ECG generation aims to recover cardiac electrical waveforms from PPG. Early methods treated this as supervised signal reconstruction, utilizing CNNs, RNNs, or Transformers [15] and specialized architectures like W-Net [31]. To enhance waveform realism, subsequent works adopted generative models. For example, CardioGAN [27] and CLEP-GAN [17] employed adversarial and contrastive learning to improve subject-independent translation. More recently, diffusion and flow-based models have driven state-of-the-art high-fidelity translation. RDDM [28] utilizes a region-disentangled diffusion process for targeted ECG components, while CardioPPG [7] generates ECGs through a tokenized frequency-domain pathway. Most closely related to our work, PPGFlowECG [10] employs a two-stage latent rectified flow, generating ECGs from a shared cross-modal latent space. Despite these advancements, existing models rely predominantly on statistical data-driven alignment, lacking explicit regularization from forward physiological dynamics.

**Physiological Simulators.** Compact mathematical models utilize low-dimensional differential equations to simulate the cardiac cycle and generate stereotyped cardiovascular waveforms [20, 8]. The canonical ECGSYN model [20], for instance, employs a three-dimensional limit-cycle oscillator with phase-locked Gaussian components to synthesize realistic P–QRS–T morphologies and heart rate variability. Similar oscillator-based frameworks have since been developed to model delayed peripheral hemodynamics, such as PPG [30]. However, purely mechanistic simulators rely on globally fixed templates, limiting their expressivity in capturing subject-specific conduction abnormalities or

complex cross-modal variations. To overcome this, recent hybrid approaches integrate physiological priors with Neural ODEs [5] or Universal Differential Equations [24]. They can enable models to preserve essential electro-hemodynamic structures while flexibly fitting real-world clinical data [26].

### 3 Method: PG-LRF

We present PG-LRF, a physiology-guided latent rectified flow framework for electro-hemodynamic PPG-to-ECG generation. PG-LRF has three components. First, an electro-hemodynamic physiological simulator co-models ECG and PPG through shared cardiac phase dynamics, an upstream ECG readout, and a delayed PPG readout. Second, a Physiology-Aware AutoEncoder (PAE) learns a modality-aware shared latent space regularized by cross-modal alignment and simulator-derived latency consistency. Third, a PPG-conditioned latent rectified flow generates ECG latents from Gaussian noise, while simulator-derived residuals guide the transport toward ECG-side morphology consistency and ECG-to-PPG forward hemodynamic consistency. The simulator and the ECG-to-PPG forward mapper are used only during training; inference requires only the input PPG.

**Problem Formulation.** Given a paired PPG segment  $\mathbf{x}_p \in \mathbb{R}^{L_p \times 1}$  and ECG segment  $\mathbf{x}_e \in \mathbb{R}^{L_e \times 1}$ , where  $L_p$  and  $L_e$  denote their native temporal lengths, our goal is to learn a conditional generator  $p(\mathbf{x}_e | \mathbf{x}_p)$  that synthesizes a plausible ECG waveform consistent with the observed PPG. The Physiology-Aware AutoEncoder maps both modalities into aligned latent representations  $\mathbf{z}_p, \mathbf{z}_e \in \mathbb{R}^{C_z \times T_z}$ , where  $C_z$  and  $T_z$  denote the latent channel dimension and temporal length. The Electro-Hemodynamic Simulator Guided Latent Rectified Flow then learns a conditional vector field  $\mathbf{v}_\psi(\mathbf{z}_t, t, \mathbf{z}_p)$  that transports a Gaussian latent variable toward the ECG latent distribution conditioned on  $\mathbf{z}_p$ . At inference time, only  $\mathbf{x}_p$  is required: we encode it into  $\mathbf{z}_p$ , solve the learned flow to obtain  $\hat{\mathbf{z}}_e$ , and decode it into the generated ECG  $\hat{\mathbf{x}}_e$ .

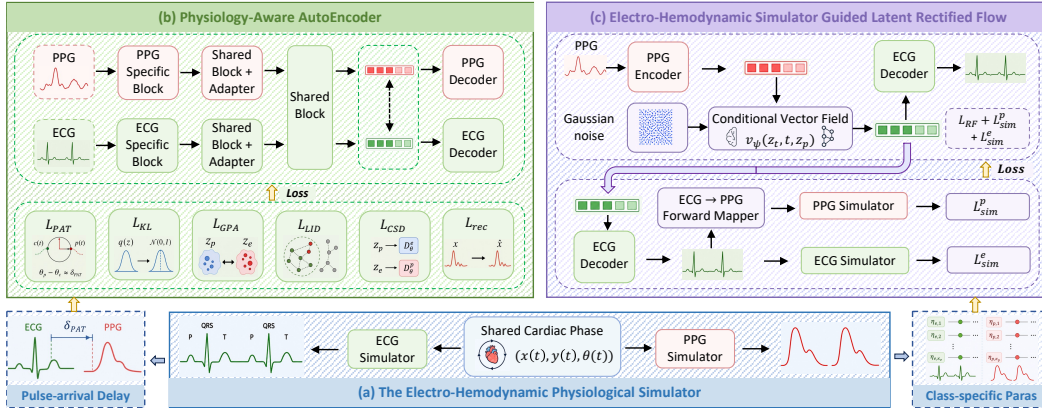


Figure 1: **Overview Framework of PG-LRF.** (a) *The Electro-Hemodynamic Physiological Simulator*: co-models ECG and PPG through shared cardiac phase dynamics. (b) *Physiology-Aware AutoEncoder*: learns an aligned electro-hemodynamic latent space from native-rate PPG and ECG. (c) *Simulator-Guided Latent Rectified Flow*: generates ECG latents conditioned on PPG and regularizes the transport with ECG morphology and ECG-to-PPG hemodynamic consistency.

#### 3.1 The Electro-Hemodynamic Physiological Simulator

Because PPG is a delayed hemodynamic response rather than a direct electrical measurement, effective PPG-to-ECG generation requires a physiological anchor that captures the asymmetric ECG-to-PPG coupling. We therefore introduce an electro-hemodynamic physiological simulator composed of four ODE functions. The functions  $f_x$  and  $f_y$  define a shared cardiac phase oscillator,  $f_e$  generates the ECG voltage readout  $e(t)$ , and  $f_p$  generates the PPG pulse readout  $p(t)$ . This simulator is not used as a rigid waveform template at inference time. Instead, it provides a soft training-time interface: the pulse-arrival delay  $\delta_{PAT}$  regularizes the PAE latent space, while the vector fields  $f_e$  and  $f_p$  define finite-difference residuals for simulator-guided latent flow training. The shared cardiac phase follows

a limit-cycle oscillator:

$$\frac{dx}{dt} = f_x(x, y) = \alpha(x, y)x - \omega y, \quad \frac{dy}{dt} = f_y(x, y) = \alpha(x, y)y + \omega x, \quad (1)$$

where  $\alpha(x, y) = 1 - \sqrt{x^2 + y^2}$  drives  $(x, y)$  toward the unit limit cycle,  $\theta(x, y) = \text{atan2}(y, x) \in [-\pi, \pi]$  denotes the cardiac phase, and  $\omega$  controls the average heart rate.

The ECG readout follows phase-locked P–QRS–T morphology:

$$\frac{de}{dt} = f_e(x, y, e, t; \eta_e) = - \sum_{\beta \in \mathcal{B}_e} a_\beta^e \Delta\theta_\beta^e(x, y) \exp\left(-\frac{(\Delta\theta_\beta^e(x, y))^2}{2(b_\beta^e)^2}\right) - [e - e_0(t)], \quad (2)$$

where  $\mathcal{B}_e = \{P, Q, R, S, T\}$  and  $\Delta\theta_\beta^e(x, y) = (\theta(x, y) - \theta_\beta^e) \bmod 2\pi$ . The parameters  $\eta_e$  collect the phase locations, amplitudes, and temporal widths of the ECG components. The PPG readout is driven by the same cardiac phase but delayed relative to the ECG R-peak:

$$\frac{dp}{dt} = f_p(x, y, p, t; \eta_p) = \sum_{\gamma \in \mathcal{B}_p} a_\gamma^p \Delta\theta_\gamma^p(x, y) \exp\left(-\frac{(\Delta\theta_\gamma^p(x, y))^2}{2(b_\gamma^p)^2}\right) - \lambda_p [p - p_0(t)], \quad (3)$$

where  $\mathcal{B}_p = \{\text{foot}, \text{sys}, \text{notch}, \text{dia}\}$  denotes the p-foot, systolic peak, diastolic notch, and diastolic wave. Its phase offset is defined as

$$\Delta\theta_\gamma^p(x, y) = (\theta(x, y) - \theta_R^e - \delta_{\text{PAT}} - \theta_\gamma^p) \bmod 2\pi, \quad (4)$$

where  $\theta_R^e$  is the ECG R-peak phase and  $\delta_{\text{PAT}}$  denotes the pulse-arrival delay from electrical activation to the peripheral pulse response. The parameters  $\eta_p$  collect  $\delta_{\text{PAT}}$ , the vascular relaxation coefficient  $\lambda_p$ , and the phase, amplitude, and width parameters of the PPG components.

**Euler Residual Interface.** We discretize the simulator on modality-specific time grids using explicit Euler updates. For modality  $m \in \{e, p\}$ , let  $\tilde{\mathbf{h}}_m$  denote a generated beat crop, let  $\mathbf{s}_{m,\ell} = (x_{m,\ell}, y_{m,\ell})$  denote the corresponding reference cardiac phase state, and let  $f_m$  be the simulator vector field with fitted parameters  $\eta_m$ . The simulator induces the finite-difference residual

$$\mathbf{r}_\ell^m = \frac{\tilde{\mathbf{h}}_{m,\ell+1} - \tilde{\mathbf{h}}_{m,\ell}}{\Delta t_m} - f_m(\mathbf{s}_{m,\ell}, \tilde{\mathbf{h}}_{m,\ell}, t_{m,\ell}; \eta_m). \quad (5)$$

Rather than enforcing the simulator as a hard waveform template, PG-LRF uses this residual as soft physiological guidance during training. The full Euler discretization and simulator fitting procedure are provided in Appendix B.1.

### 3.2 Physiology-Aware AutoEncoder

The Physiology-Aware AutoEncoder (PAE) learns a shared cardiovascular latent space for paired PPG and ECG signals while preserving modality-specific acquisition characteristics. As shown in Figure 1, the encoder adopts a modality-specific-to-shared design. PPG and ECG are first processed by modality-specific blocks that preserve acquisition-dependent characteristics, such as waveform morphology, frequency content, and noise patterns. The resulting representations are then passed through shared blocks to extract common cardiovascular factors. To avoid losing useful modality-dependent information during shared abstraction, we insert lightweight modality-aware adapters in the intermediate shared blocks. A final shared bottleneck maps both modalities to a common latent posterior space. For modality  $m \in \{p, e\}$ , let  $\mathbf{h}_m^{(0)} = \mathbf{x}_m$ . The modality-specific blocks are defined as

$$\mathbf{h}_m^{(i)} = F_{m,i}^{\text{spec}}(\mathbf{h}_m^{(i-1)}), \quad i = 1, 2, \quad (6)$$

where  $F_{m,i}^{\text{spec}}$  denotes the  $i$ -th modality-specific block for modality  $m$ . The intermediate shared blocks with modality-aware adapters are then written as

$$\mathbf{u}_m^{(k)} = F_k^{\text{sh}}(\mathbf{h}_m^{(k-1)}), \quad \mathbf{h}_m^{(k)} = \mathbf{u}_m^{(k)} + A_{m,k}(\mathbf{u}_m^{(k)}), \quad k = 3, \dots, 5, \quad (7)$$

where  $F_k^{\text{sh}}$  is the  $k$ -th shared block and  $A_{m,k}$  is the modality-aware adapter. The final shared bottleneck is

$$\mathbf{h}_m^{(6)} = F_6^{\text{sh}}(\mathbf{h}_m^{(5)}). \quad (8)$$

The encoder parameterizes a diagonal Gaussian posterior by

$$[\boldsymbol{\mu}_m, \log \boldsymbol{\sigma}_m^2] = H_\phi(\mathbf{h}_m^{(6)}), \quad q_\phi^m(\mathbf{z}_m | \mathbf{x}_m) = \mathcal{N}(\boldsymbol{\mu}_m, \text{diag}(\boldsymbol{\sigma}_m^2)), \quad (9)$$

and samples the latent representation as

$$\mathbf{z}_m = \boldsymbol{\mu}_m + \boldsymbol{\sigma}_m \odot \boldsymbol{\epsilon}, \quad \boldsymbol{\epsilon} \sim \mathcal{N}(\mathbf{0}, \mathbf{I}). \quad (10)$$

Here  $\boldsymbol{\mu}_m, \log \boldsymbol{\sigma}_m^2 \in \mathbb{R}^{C_z \times T_z}$ , so both PPG and ECG are mapped into aligned latent representations  $\mathbf{z}_p, \mathbf{z}_e \in \mathbb{R}^{C_z \times T_z}$ . The decoder for each modality reconstructs the waveform at its native temporal length. It contains a residual reconstruction branch and a lightweight decomposition branch:

$$\hat{\mathbf{x}}_m = D_\theta^m(\mathbf{z}_m) = D_{\text{res}}^m(\mathbf{z}_m) + D_{\text{dec}}^m(\mathbf{z}_m), \quad (11)$$

where

$$D_{\text{dec}}^m(\mathbf{z}_m) = D_{\text{level}}^m(\mathbf{z}_m) + D_{\text{trend}}^m(\mathbf{z}_m) + D_{\text{season}}^m(\mathbf{z}_m). \quad (12)$$

The residual branch models local waveform morphology, while the decomposition branch provides a lightweight bias for global level, slow temporal drift, and coarse recurrent structure.

**PAE Training Objective.** PAE is optimized with three groups of objectives: native-rate autoencoding, cross-modal latent alignment, and simulator-informed delay consistency.

(i) *Simulator-informed phase delay consistency.* PPG is a delayed hemodynamic response to ECG activation. Therefore, the phase gap between the generated ECG and PPG should be consistent with the class-specific simulator delay  $\delta_{\text{PAT}}$ . Let  $\hat{\mathbf{x}}_e = D_\theta^e(\mathbf{z}_e)$ , and  $\hat{\mathbf{x}}_p = D_\theta^p(\mathbf{z}_p)$ , where  $\hat{\mathbf{x}}_e$  and  $\hat{\mathbf{x}}_p$  are the reconstructed ECG and PPG waveforms. Let  $\Theta_e(\cdot)$  estimate the ECG activation phase and  $\Theta_p(\cdot)$  estimate the PPG pulse phase. The estimated electro-hemodynamic phase delay is  $\widehat{\Delta\theta}_{\text{PAT}} = \text{wrap}_\pi(\Theta_p(\hat{\mathbf{x}}_p) - \Theta_e(\hat{\mathbf{x}}_e))$ , where  $\text{wrap}_\pi(\cdot)$  maps the phase difference to  $[-\pi, \pi]$ . Since phase is circular, we use a circular squared distance:  $d_{\text{circ}}(a, b) = [\text{atan2}(\sin(a - b), \cos(a - b))]^2$ . The phase delay consistency loss is then

$$\mathcal{L}_{\text{PAT}} = \frac{1}{B} \sum_{i=1}^B d_{\text{circ}}\left(\widehat{\Delta\theta}_{\text{PAT}}^{(i)}, \delta_{\text{PAT}}^{(i)}\right). \quad (13)$$

(ii) *Autoencoding regularization.* The reconstruction loss preserves modality-specific waveform information:

$$\mathcal{L}_{\text{rec}} = \|D_\theta^p(\mathbf{z}_p) - \mathbf{x}_p\|_2^2 + \|D_\theta^e(\mathbf{z}_e) - \mathbf{x}_e\|_2^2. \quad (14)$$

The KL term regularizes both modality posteriors toward a standard Gaussian prior:

$$\mathcal{L}_{\text{KL}} = D_{\text{KL}}\left(q_\phi^p(\mathbf{z}_p | \mathbf{x}_p) \| \mathcal{N}(\mathbf{0}, \mathbf{I})\right) + D_{\text{KL}}\left(q_\phi^e(\mathbf{z}_e | \mathbf{x}_e) \| \mathcal{N}(\mathbf{0}, \mathbf{I})\right). \quad (15)$$

(iii) *Cross-modal latent alignment.* We align paired PPG and ECG representations at both distribution and instance levels. Global posterior alignment matches posterior means and dispersion:

$$\mathcal{L}_{\text{GPA}} = \|\boldsymbol{\mu}_e - \boldsymbol{\mu}_p\|_2^2 + \frac{1}{2} \left[ D_{\text{KL}}\left(q_\phi^e(\mathbf{z}_e | \mathbf{x}_e) \| q_\phi^p(\mathbf{z}_p | \mathbf{x}_p)\right) + D_{\text{KL}}\left(q_\phi^p(\mathbf{z}_p | \mathbf{x}_p) \| q_\phi^e(\mathbf{z}_e | \mathbf{x}_e)\right) \right]. \quad (16)$$

To preserve instance-level distinctions, we use a bidirectional contrastive loss. Let  $\bar{\mathbf{z}}_m^{(i)}$  denote the normalized pooled latent of the  $i$ -th sample from modality  $m$ , and define  $s(\mathbf{a}, \mathbf{b}) = \exp(\langle \mathbf{a}, \mathbf{b} \rangle / \tau)$ .

$$\mathcal{L}_{\text{LID}} = -\frac{1}{2B} \sum_{i=1}^B \left[ \log \frac{s(\bar{\mathbf{z}}_p^{(i)}, \bar{\mathbf{z}}_e^{(i)})}{\sum_{j=1}^B s(\bar{\mathbf{z}}_p^{(i)}, \bar{\mathbf{z}}_e^{(j)})} + \log \frac{s(\bar{\mathbf{z}}_e^{(i)}, \bar{\mathbf{z}}_p^{(i)})}{\sum_{j=1}^B s(\bar{\mathbf{z}}_e^{(i)}, \bar{\mathbf{z}}_p^{(j)})} \right]. \quad (17)$$

Finally, we use a weak cross-modal decodability objective to encourage each latent to retain modality-shared physiological information. And this objective is assigned a small weight and is intended only as a weak physiological decodability constraint.

$$\mathcal{L}_{\text{CSD}} = \|D_\theta^e(\mathbf{z}_p) - \mathbf{x}_e\|_2^2 + \|D_\theta^p(\mathbf{z}_e) - \mathbf{x}_p\|_2^2. \quad (18)$$

The full PAE objective is

$$\mathcal{L}_{\text{PAE}} = \lambda_{\text{PAT}} \mathcal{L}_{\text{PAT}} + \mathcal{L}_{\text{rec}} + \beta \mathcal{L}_{\text{KL}} + \lambda_{\text{GPA}} \mathcal{L}_{\text{GPA}} + \lambda_{\text{LID}} \mathcal{L}_{\text{LID}} + \lambda_{\text{CSD}} \mathcal{L}_{\text{CSD}}. \quad (19)$$

After PAE training, the PPG encoder, ECG encoder, and ECG decoder are frozen for the subsequent PPG-conditioned latent rectified flow.

### 3.3 Electro-Hemodynamic Simulator Guided Latent Rectified Flow

After PAE training, we freeze the PPG encoder, ECG encoder, and ECG decoder. For each paired sample, we obtain the PPG condition latent  $\mathbf{z}_p = E_\phi^p(\mathbf{x}_p)$  and the target ECG latent  $\mathbf{z}_e = E_\phi^e(\mathbf{x}_e)$ . Following latent rectified flow [10], we learn a conditional vector field that transports Gaussian noise toward the ECG latent distribution conditioned on  $\mathbf{z}_p$ . Given  $\mathbf{z}_0 \sim \mathcal{N}(\mathbf{0}, \mathbf{I})$  and  $t \sim \mathcal{U}(0, 1)$ , we define the linear interpolation path

$$\mathbf{z}_t = (1 - t)\mathbf{z}_0 + t\mathbf{z}_e, \quad (20)$$

and optimize the flow-matching objective

$$\mathcal{L}_{\text{RF}} = \mathbb{E} \left[ \|\mathbf{v}_\psi(\mathbf{z}_t, t, \mathbf{z}_p) - (\mathbf{z}_e - \mathbf{z}_0)\|_2^2 \right]. \quad (21)$$

The vector field  $\mathbf{v}_\psi$  is parameterized by a conditional Transformer, where the evolving ECG latent attends to the PPG condition latent through cross-attention. To further constrain the generated ECG with electro-hemodynamic dynamics, we apply simulator guidance only to the terminal generated state rather than to every intermediate flow state. This avoids unstable gradients from early noisy latent states and aligns the physiological regularization with the final ECG waveform used at inference. Given a noise latent  $\mathbf{z}_0$ , we obtain a differentiable terminal estimate by integrating the learned vector field with  $K$  Euler steps:

$$\tilde{\mathbf{z}}_{k+1} = \tilde{\mathbf{z}}_k + \Delta\tau v_\psi(\tilde{\mathbf{z}}_k, \tau_k, \mathbf{z}_p), \quad \tau_k = \frac{k}{K}, \quad \Delta\tau = \frac{1}{K}, \quad \tilde{\mathbf{z}}_e = \tilde{\mathbf{z}}_K, \quad \tilde{\mathbf{x}}_e = D_\theta^e(\tilde{\mathbf{z}}_e). \quad (22)$$

The decoded terminal ECG  $\tilde{\mathbf{x}}_e$  is then used to compute simulator-informed residual losses.

**ECG-to-PPG Forward Mapper.** The generated ECG should not only exhibit plausible electrical morphology, but also induce a plausible delayed hemodynamic response. We therefore use a lightweight ECG-to-PPG forward mapper  $G_\rho$  as a differentiable bridge from the decoded ECG domain to the PPG signal domain:

$$\tilde{\mathbf{x}}_p = G_\rho(\tilde{\mathbf{x}}_e). \quad (23)$$

The mapper is implemented as a small temporal convolutional network with residual 1D convolution blocks and a final temporal resizing layer. It is pretrained on paired real ECG–PPG segments with waveform and derivative reconstruction losses, and then frozen during latent flow training. It is used only for training-time physiological regularization and is not required at inference.

**Simulator-guided Residual Losses.** To capture heterogeneous electro-hemodynamic patterns, we fit simulator parameters using ICD-stratified training groups. For each group  $\kappa$ , we estimate  $\eta^\kappa = (\eta_e^\kappa, \eta_p^\kappa)$  from representative ECG–PPG beats and use them only to construct training-time simulator residuals. These labels are not used as model inputs, and PG-LRF requires only PPG at inference time. Let  $\mathcal{C}_e(\tilde{\mathbf{x}}_e^t) = \tilde{\mathbf{h}}_e \in \mathbb{R}^{L_e^c}$  denote a QRS-aligned generated ECG beat crop. Given fitted ECG simulator parameters  $\eta_e^\kappa$  and reference phase states  $(x_{e,\ell}^\kappa, y_{e,\ell}^\kappa)$ , we penalize deviations from the ECG vector field by the Euler residual:

$$\mathcal{L}_{\text{sim}}^e = \frac{1}{L_e^c - 1} \sum_{\ell=1}^{L_e^c-1} \left\| \frac{\tilde{h}_{e,\ell+1} - \tilde{h}_{e,\ell}}{\Delta t_e} - f_e \left( x_{e,\ell}^\kappa, y_{e,\ell}^\kappa, \tilde{h}_{e,\ell}, t_{e,\ell}; \eta_e^\kappa \right) \right\|_2^2. \quad (24)$$

This term encourages generated ECG beats to follow physiologically plausible P–QRS–T dynamics rather than only matching point-wise waveform statistics.

Similarly, let  $\mathcal{C}_p(\tilde{\mathbf{x}}_p^t) = \tilde{\mathbf{h}}_p \in \mathbb{R}^{L_p^c}$  denote the induced PPG beat crop. Given fitted PPG simulator parameters  $\eta_p^\kappa$  and reference phase states  $(x_{p,\ell}^\kappa, y_{p,\ell}^\kappa)$ , we define

$$\mathcal{L}_{\text{sim}}^p = \frac{1}{L_p^c - 1} \sum_{\ell=1}^{L_p^c-1} \left\| \frac{\tilde{h}_{p,\ell+1} - \tilde{h}_{p,\ell}}{\Delta t_p} - f_p \left( x_{p,\ell}^\kappa, y_{p,\ell}^\kappa, \tilde{h}_{p,\ell}, t_{p,\ell}; \eta_p^\kappa \right) \right\|_2^2. \quad (25)$$

This term regularizes the generated ECG through its induced PPG response, encouraging compatibility with delayed peripheral pulse dynamics.

The complete simulator-guided flow objective is

$$\mathcal{L}_{\text{Flow}} = \mathcal{L}_{\text{RF}} + \lambda_e \mathcal{L}_{\text{sim}}^e + \lambda_p \mathcal{L}_{\text{sim}}^p. \quad (26)$$

The simulator-informed losses and the ECG-to-PPG forward mapper are used only during training. At inference time, the model only requires the PPG input, solves the learned latent flow, and decodes the generated ECG latent through the frozen ECG decoder.

### 3.4 Training and Inference

PG-LRF is optimized in two phases. We first train the Physiology-Aware AutoEncoder with the objective  $\mathcal{L}_{\text{PAE}}$  to obtain aligned PPG and ECG latent representations. Afterward, we freeze the PPG encoder, ECG encoder, and ECG decoder, and train only the PPG-conditioned latent rectified flow. The simulator-informed terms are used only during training and do not change the inference procedure. At inference time, only the PPG input is required. Given  $\mathbf{x}_p$ , we compute the condition latent  $\mathbf{z}_p = E_{\phi}^p(\mathbf{x}_p)$ , sample  $\mathbf{z}_0 \sim \mathcal{N}(\mathbf{0}, \mathbf{I})$ , and solve the learned ODE  $d\mathbf{z}_t/dt = \mathbf{v}_{\psi}(\mathbf{z}_t, t, \mathbf{z}_p)$  from  $t = 0$  to  $t = 1$ . With an Euler solver using  $N$  steps and step size  $\Delta t = 1/N$ , the update is

$$\mathbf{z}_{k+1} = \mathbf{z}_k + \Delta t \mathbf{v}_{\psi}(\mathbf{z}_k, t_k, \mathbf{z}_p), \quad k = 0, \dots, N - 1. \quad (27)$$

The final latent  $\mathbf{z}_N$  is decoded by the frozen ECG decoder to obtain the generated ECG waveform:

$$\hat{\mathbf{x}}_e = D_{\theta}^e(\mathbf{z}_N). \quad (28)$$

## 4 Experiments

**Dataset and Preprocessing.** We evaluate PG-LRF on MC-MED [13], a large-scale multimodal clinical monitoring dataset comprising 118,385 adult emergency department visits from 70,545 unique patients at Stanford Health Care between 2020 and 2022. This dataset provides continuous, temporally synchronized physiological waveforms—specifically electrocardiography (ECG) and photoplethysmography (PPG)—alongside visit-level clinical metadata. From these continuous recordings, we extract synchronized 10-second paired windows of PPG and ECG. To preserve acquisition-specific temporal structures, we maintain both modalities at their native sampling rates: 40 Hz for PPG (yielding  $\mathbf{x}_p \in \mathbb{R}^{400 \times 1}$ ) and 120 Hz for ECG (yielding  $\mathbf{x}_e \in \mathbb{R}^{1200 \times 1}$ ). Prior to modeling, we apply z-score normalization to each segment. Finally, to ensure signal integrity, we explicitly exclude any windows exhibiting missing values, severe truncation, or invalid signal lengths. We follow the official MC-MED training and testing data splits to ensure fair comparison.

**Baseline.** We compare PG-LRF with four baselines covering adversarial, diffusion-based, raw-space flow, and latent-flow paradigms. (i) *CardioFlow* [22] formulates PPG-to-ECG translation as a rectified-flow generation problem in the waveform space. (ii) *RDDM* [28] is a diffusion-based model that separately handles ECG regions of interest, such as QRS complexes, and non-ROI regions. (iii) *CardioGAN* [27] uses an attention-based generator with time- and frequency-domain discriminators. (iv) *PPGFlowECG* [10] first aligns PPG and ECG in a shared latent space and then performs PPG-conditioned latent rectified flow. All baselines are adapted to our MC-MED setting and evaluated under the same data split, preprocessing pipeline, and metrics.

**Ablation Study.** To isolate the impact of our core physiological designs, we evaluate PG-LRF against two ablated variants: (i) *PG-LRF w/o Sim*: We remove all simulator guidance during latent flow training. This reduces the model to a purely data-driven flow, demonstrating the necessity of explicit physiological regularization. (ii) *PG-LRF w/o PAE*: We replace our modality-specific-to-shared PAE architecture with two separate standard autoencoders. This validates the importance of progressively mapping acquisition-specific structures into a shared cardiovascular latent space rather than processing modalities entirely independently.

### 4.1 ECG Generation Performance

We evaluate ECG generation quality from two complementary perspectives: waveform-level fidelity and morphology-level physiological consistency. The first evaluation compares the generated ECG  $\hat{\mathbf{x}}_e$  with the paired ground-truth ECG  $\mathbf{x}_e$  at the whole-signal level, while the second evaluation examines whether clinically meaningful fiducial intervals and morphology measurements are preserved.

**Waveform-level fidelity.** We evaluate waveform fidelity using point-wise metrics (MAE and RMSE), distribution-level metrics (FD and FID), and heart-rate consistency (HR MAE). All results are reported as mean  $\pm$  standard deviation over three runs. As shown in Table 1, PG-LRF achieves the best performance across all metrics. Compared with the strongest baseline PPGFlowECG, PG-LRF reduces MAE from 0.87 to 0.71, RMSE from 1.32 to 1.07, FID from 44.17 to 37.79, and HR MAE from 7.08 to 3.94, indicating better waveform reconstruction, distributional realism, and rhythm consistency. The ablation results further support the contribution of each component. Removing

simulator guidance degrades MAE, RMSE, FID, and HR MAE, showing that physiological constraints improve waveform realism and beat-rate consistency. Replacing the PAE with separate standard autoencoders also worsens performance, especially on FD and HR MAE, suggesting that the aligned electro-hemodynamic latent space is important for PPG-conditioned ECG generation.

Table 1: ECG generation performance on MC-MED. Lower values indicate better performance. Results are reported as mean  $\pm$  standard deviation over three runs.

Method	MAE $\downarrow$	RMSE $\downarrow$	FD $\downarrow$	FID $\downarrow$	HR MAE $\downarrow$
RDDM	0.95 $\pm$ 0.01	1.41 $\pm$ 0.01	60.34 $\pm$ 0.47	47.97 $\pm$ 0.12	5.48 $\pm$ 0.08
CardioGAN	1.07 $\pm$ 0.01	1.46 $\pm$ 0.01	74.17 $\pm$ 0.22	47.01 $\pm$ 0.01	4.71 $\pm$ 0.01
CardioFlow	0.94 $\pm$ 0.01	1.35 $\pm$ 0.01	58.78 $\pm$ 0.65	86.77 $\pm$ 0.22	6.83 $\pm$ 0.74
PPGFlowECG	0.87 $\pm$ 0.04	1.32 $\pm$ 0.04	46.64 $\pm$ 1.49	44.17 $\pm$ 0.11	7.08 $\pm$ 0.10
<b>PG-LRF</b>	<b>0.71 <math>\pm</math> 0.04</b>	<b>1.07 <math>\pm</math> 0.05</b>	<b>39.68 <math>\pm</math> 1.96</b>	<b>37.79 <math>\pm</math> 0.27</b>	<b>3.94 <math>\pm</math> 0.76</b>
w/o Sim	0.84 $\pm$ 0.01	1.28 $\pm$ 0.01	40.51 $\pm$ 1.20	45.90 $\pm$ 0.27	4.94 $\pm$ 0.57
w/o PAE	0.85 $\pm$ 0.05	1.26 $\pm$ 0.01	43.10 $\pm$ 0.88	44.07 $\pm$ 0.37	6.36 $\pm$ 0.07

**Morphology and interval fidelity.** Beyond global waveform similarity, we evaluate whether the generated ECG preserves clinically meaningful fiducial measurements. We report the MAE of PR interval, QRS duration, QT interval, QTcF, ST-J60 deviation, P-wave duration, and T-wave duration between generated and real ECGs. As shown in Table 2, PG-LRF achieves the best performance across all metrics. Compared with PPGFlowECG, PG-LRF reduces PR error from 68.9 to 59.9 ms, QRS error from 48.1 to 38.6 ms, QT error from 32.5 to 29.3 ms, and QTcF error from 35.9 to 32.2 ms. It also improves ST-J60 deviation and both P- and T-wave duration errors, indicating that the generated ECGs better preserve conduction, depolarization, and ST-segment morphology.

Table 2: Morphology and interval fidelity on MC-MED. We report the MAE of each fiducial measurement between generated and real ECGs. Interval metrics are reported in milliseconds, and ST-J60 deviation is reported in normalized amplitude units. Lower values indicate better performance.

Method	PR $\downarrow$	QRS $\downarrow$	QT $\downarrow$	QTcF $\downarrow$	ST-J60 $\downarrow$	P dur. $\downarrow$	T dur. $\downarrow$
RDDM	66.3 $\pm$ 0.4	39.2 $\pm$ 1.1	40.7 $\pm$ 0.6	43.8 $\pm$ 0.6	0.22 $\pm$ 0.0	19.6 $\pm$ 0.2	22.3 $\pm$ 0.1
CardioGAN	65.2 $\pm$ 0.6	43.0 $\pm$ 0.4	56.3 $\pm$ 0.8	61.5 $\pm$ 0.9	0.36 $\pm$ 0.02	27.6 $\pm$ 0.3	24.7 $\pm$ 0.2
CardioFlow	75.8 $\pm$ 1.5	56.8 $\pm$ 0.6	73.9 $\pm$ 1.4	81.1 $\pm$ 1.3	0.20 $\pm$ 0.01	52.8 $\pm$ 0.1	38.9 $\pm$ 0.2
PPGFlowECG	68.9 $\pm$ 0.5	48.1 $\pm$ 0.3	32.5 $\pm$ 0.3	35.9 $\pm$ 0.3	0.16 $\pm$ 0.01	28.8 $\pm$ 0.2	37.7 $\pm$ 0.2
<b>PG-LRF</b>	<b>59.9 <math>\pm</math> 0.9</b>	<b>38.6 <math>\pm</math> 0.5</b>	<b>29.3 <math>\pm</math> 0.6</b>	<b>32.2 <math>\pm</math> 0.5</b>	<b>0.14 <math>\pm</math> 0.02</b>	<b>19.3 <math>\pm</math> 0.4</b>	<b>21.3 <math>\pm</math> 0.4</b>

## 4.2 Cardiovascular Disease Detection

To assess whether the generated ECGs preserve clinically useful information, we evaluate downstream multi-label cardiovascular disease detection. Following prior PPG-to-ECG benchmarks, we use visit-level ICD-based cardiovascular labels, including I48, I71, I70, I44, I25, and I50, covering rhythm, conduction, vascular, ischemic, and heart-failure-related conditions.

Table 3: Quantitative evaluation of multi-label cardiovascular disease classification on the MC-MED dataset. We compare a PPG-based baseline, and PG-LRF. Higher AUROC indicates better performance.

Methods	Disease Categories (AUROC) $\uparrow$						Macro-AUROC $\uparrow$
	I48	I71	I70	I44	I25	I50	
PaPaGei	0.525 $\pm$ 0.03	0.521 $\pm$ 0.11	0.513 $\pm$ 0.03	0.653 $\pm$ 0.11	0.528 $\pm$ 0.07	0.520 $\pm$ 0.03	0.545 $\pm$ 0.04
<b>PG-LRF</b>	<b>0.697 <math>\pm</math> 0.01</b>	<b>0.610 <math>\pm</math> 0.02</b>	<b>0.622 <math>\pm</math> 0.02</b>	<b>0.656 <math>\pm</math> 0.03</b>	<b>0.665 <math>\pm</math> 0.01</b>	<b>0.551 <math>\pm</math> 0.02</b>	<b>0.633 <math>\pm</math> 0.01</b>

As shown in Table 3, ECGs generated by PG-LRF achieve higher AUROC than the PPG-based PaPaGei baseline across all disease categories, improving Macro-AUROC from 0.545 to 0.633. The gains are particularly clear for I48, I70, and I25, suggesting that the generated ECGs recover clinically relevant electrical patterns that are less accessible from raw PPG alone. We use the same data split and classifier architecture across all settings. Since the labels are visit-level ICD codes

rather than ECG-only diagnostic annotations, this experiment is intended as a downstream clinical utility evaluation rather than evidence for standalone diagnostic deployment.

### 4.3 Qualitative Case Studies.

Figure 2 presents three representative qualitative examples of PPG-to-ECG generation by PG-LRF. Across all cases, the generated ECGs are well aligned with the observed PPG in beat timing and overall rhythm, while recovering morphologies close to the reference ECGs.

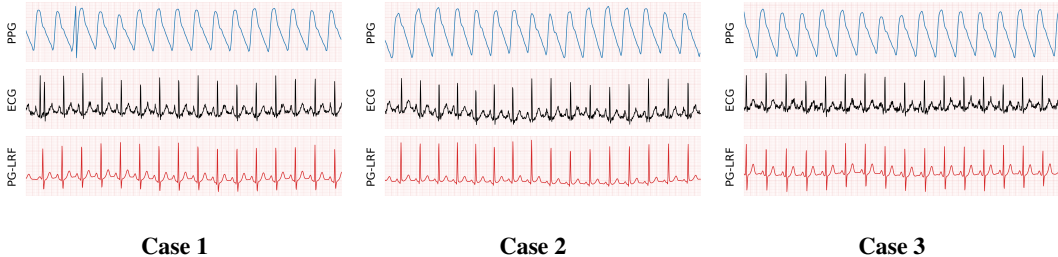


Figure 2: Qualitative case studies of PPG-to-ECG generation by PG-LRF. Across the three cases, PG-LRF produces ECG that are visually consistent with the reference ECG in overall rhythm, major waveform morphology, and beat timing, while remaining compatible with the observed PPG.

In Case 1, the reference ECG contains noticeable noise, but PG-LRF still preserves the main rhythm and QRS structure, suggesting good robustness to nuisance variation. In Case 2, the reference ECG shows clear beat-to-beat variation, which is also reflected in the generated ECG, indicating that PG-LRF captures underlying rhythm dynamics rather than only an average waveform pattern. In Case 3, PG-LRF again preserves realistic rhythm regularity and the main P–QRS–T morphology, while producing a smoother but still clinically plausible ECG. Overall, these examples complement the quantitative results by showing that PG-LRF preserves both global temporal organization and local waveform details under PPG-conditioned generation.

## 5 Broader impacts

PG-LRF may have positive impacts for scalable cardiovascular monitoring. Since PPG is widely available in wearable devices and bedside monitors, generating ECG-like signals from PPG could support research on long-term cardiac monitoring, data augmentation, and retrospective analysis when ECG is unavailable or difficult to collect continuously. The proposed physiology-guided framework may also encourage more clinically grounded generative modeling for physiological time series.

## 6 Conclusion

In this paper, we presented PG-LRF, a physiology-guided latent rectified flow framework designed to overcome the limitations of purely data-driven PPG-to-ECG generation. Rather than treating this task as a simple statistical cross-modal translation, PG-LRF explicitly grounds the generative process in the underlying cardiovascular dynamics. We introduced a novel electro-hemodynamic simulator that co-models ECG and PPG via shared cardiac phase dynamics. This simulator provides soft, phase-aware guidance to a native-rate Physiology-Aware AutoEncoder to structure the latent space, and explicitly regularizes the latent rectified flow to enforce both ECG-side morphological fidelity and forward ECG-to-PPG hemodynamic consistency. Extensive evaluations on the large-scale MC-MED dataset demonstrate that PG-LRF consistently outperforms existing baselines, generating ECGs that are not only signal-faithful but also preserve critical clinical intervals and improve downstream cardiovascular disease classification. Ultimately, PG-LRF effectively bridges the gap between ubiquitous wearable sensing and verifiable clinical cardiac assessment, demonstrating the profound value of integrating mechanistic physiological priors with modern latent generative modeling.

## References

- [1] John Allen. Photoplethysmography and its application in clinical physiological measurement. *Physiological measurement*, 28(3):R1–R39, 2007.
- [2] Selcan Kaplan Berkaya, Alper Kursat Uysal, Efnan Sora Gunal, Semih Ergin, Serkan Gunal, and M Bilginer Gulmezoglu. A survey on ecg analysis. *Biomedical Signal Processing and Control*, 43:216–235, 2018.
- [3] Denisse Castaneda, Aibhlin Esparza, Mohammad Ghamari, Cinna Soltanpur, and Homer Nazeran. A review on wearable photoplethysmography sensors and their potential future applications in health care. *International journal of biosensors & bioelectronics*, 4(4):195, 2018.
- [4] Peter H Charlton, Panicos A Kyriacou, Jonathan Mant, Vaidotas Marozas, Phil Chowienczyk, and Jordi Alastruey. Wearable photoplethysmography for cardiovascular monitoring. *Proceedings of the IEEE*, 110(3):355–381, 2022.
- [5] Ricky T. Q. Chen, Yulia Rubanova, Jesse Bettencourt, and David Duvenaud. Neural ordinary differential equations. In *Advances in Neural Information Processing Systems (NeurIPS)*, 2018.
- [6] Florinel-Alin Croitoru, Vlad Hondru, Radu Tudor Ionescu, and Mubarak Shah. Diffusion models in vision: A survey. *IEEE transactions on pattern analysis and machine intelligence*, 45(9):10850–10869, 2023.
- [7] Zhengyao Ding, Yujian Hu, Ziyu Li, Yiheng Mao, Haitao Li, Dongchen Zhou, Xuesen Chu, Long Yu, Ziyi Liu, Fei Wu, et al. Ai modeling photoplethysmography to electrocardiography useful for predicting cardiovascular disease. *npj Digital Medicine*, 2025.
- [8] Jan-Christoph Edelmann, Dominik Mair, Daniel Ziesel, Martin Burtscher, and Thomas Ussmueller. An ecg simulator with a novel ecg profile for physiological signals. *Journal of medical engineering & technology*, 42(7):501–509, 2018.
- [9] Patrick Esser, Sumith Kulal, Andreas Blattmann, Rahim Entezari, Jonas Müller, Harry Saini, Yam Levi, Dominik Lorenz, Axel Sauer, Frederic Boesel, et al. Scaling rectified flow transformers for high-resolution image synthesis. In *Forty-first international conference on machine learning*, 2024.
- [10] Xiaocheng Fang, Jiarui Jin, Haoyu Wang, Che Liu, Jieyi Cai, Yujie Xiao, Guangkun Nie, Bo Liu, Shun Huang, Hongyan Li, et al. Ppgflowecg: Latent rectified flow with cross-modal encoding for ppg-guided ecg generation and cardiovascular disease detection. *arXiv preprint arXiv:2509.19774*, 2025.
- [11] Jesse Fine, Kimberly L Branan, Andres J Rodriguez, Tananant Boonya-Ananta, Ajmal, Jessica C Ramella-Roman, Michael J McShane, and Gerard L Cote. Sources of inaccuracy in photoplethysmography for continuous cardiovascular monitoring. *Biosensors*, 11(4):126, 2021.
- [12] Jonathan Ho, Ajay Jain, and Pieter Abbeel. Denoising diffusion probabilistic models. *Advances in neural information processing systems*, 33:6840–6851, 2020.
- [13] Aman Kansal, Emma Chen, Tom Jin, Pranav Rajpurkar, and David Kim. Multimodal clinical monitoring in the emergency department (mc-med). *Published online March*, 3, 2025.
- [14] Paul Kligfield, Leonard S Gettes, James J Bailey, Rory Childers, Barbara J Deal, E. William Hancock, Gerard van Herpen, Jan A Kors, Peter Macfarlane, David M Mirvis, and et al. Recommendations for the standardization and interpretation of the electrocardiogram: Part i: The electrocardiogram and its technology. *Circulation*, 115(10):1306–1324, 2007.
- [15] Ella Lan. Performer: A novel ppg-to-ecg reconstruction transformer for a digital biomarker of cardiovascular disease detection. In *Proceedings of the IEEE/CVF Winter Conference on Applications of Computer Vision*, pages 1991–1999, 2023.
- [16] Sangyun Lee, Zinan Lin, and Giulia Fanti. Improving the training of rectified flows. *Advances in neural information processing systems*, 37:63082–63109, 2024.

- [17] Xiaoyan Li, Shixin Xu, Faisal Habib, Neda Aminnejad, Arvind Gupta, and Huaxiong Huang. Clep-gan: an innovative approach to subject-independent ecg reconstruction from ppg signals. *BMC bioinformatics*, 26(1):306, 2025.
- [18] Zhiyuan Li, Yuanyuan Tian, Yanrui Jin, Xiaoyang Wei, Mengxiao Wang, Jinlei Liu, and Chengliang Liu. Eddm: A novel ecg denoising method using dual-path diffusion model. *IEEE Transactions on Instrumentation and Measurement*, 2025.
- [19] Yaron Lipman, Ricky TQ Chen, Heli Ben-Hamu, Maximilian Nickel, and Matthew Le. Flow matching for generative modeling. In *The Eleventh International Conference on Learning Representations*, 2023.
- [20] Patrick E McSharry, Gari D Clifford, Lionel Tarassenko, and Leonard A Smith. A dynamical model for generating synthetic electrocardiogram signals. *IEEE transactions on biomedical engineering*, 50(3):289–294, 2003.
- [21] Volodymyr Mnih, Koray Kavukcuoglu, David Silver, Alex Graves, Ioannis Antonoglou, Daan Wierstra, and Martin Riedmiller. Playing atari with deep reinforcement learning. *arXiv preprint arXiv:1312.5602*, 2013.
- [22] Yuta Nambu, Masahiro Kohjima, and Ryuji Yamamoto. Cardioflow: Learning to generate ecg from ppg with rectified flow. In *ICASSP 2025-2025 IEEE International Conference on Acoustics, Speech and Signal Processing (ICASSP)*, pages 1–5. IEEE, 2025.
- [23] Wei Qian, Gaoji Su, Dan Guo, Jinxing Zhou, Xiaobai Li, Bin Hu, Shengeng Tang, and Meng Wang. Physdiff: physiology-based dynamicity disentangled diffusion model for remote physiological measurement. In *Proceedings of the AAAI Conference on Artificial Intelligence*, volume 39, pages 6568–6576, 2025.
- [24] Christopher Rackauckas, Yingbo Ma, Julius Martensen, Collin Warner, Kirill Zubov, Rohit Supekar, Dominic Skinner, Ali Ramadhan, and Alan Edelman. Universal differential equations for scientific machine learning. *arXiv preprint arXiv:2001.04385*, 2020.
- [25] Robin Rombach, Andreas Blattmann, Dominik Lorenz, Patrick Esser, and Björn Ommer. High-resolution image synthesis with latent diffusion models. In *Proceedings of the IEEE/CVF conference on computer vision and pattern recognition*, pages 10684–10695, 2022.
- [26] Yuling Sang, Abhirup Banerjee, Marcel Beetz, and Vicente Grau. Deep conditional generative model for personalization of 12-lead electrocardiograms and cardiovascular risk prediction. *Frontiers in Digital Health*, 7:1558589, 2025.
- [27] Pritam Sarkar and Ali Etemad. Cardiogan: Attentive generative adversarial network with dual discriminators for synthesis of ecg from ppg. In *Proceedings of the AAAI Conference on Artificial Intelligence*, volume 35, pages 488–496, 2021.
- [28] Debaditya Shome, Pritam Sarkar, and Ali Etemad. Region-disentangled diffusion model for high-fidelity ppg-to-ecg translation. In *Proceedings of the AAAI conference on artificial intelligence*, volume 38, pages 15009–15019, 2024.
- [29] George Stoica, Vivek Ramanujan, Xiang Fan, Ali Farhadi, Ranjay Krishna, and Judy Hoffman. Contrastive flow matching. In *Proceedings of the IEEE/CVF International Conference on Computer Vision*, pages 1185–1194, 2025.
- [30] Qunfeng Tang, Zhencheng Chen, Rabab Ward, and Mohamed Elgendi. Synthetic photoplethysmogram generation using two gaussian functions. *Scientific Reports*, 10(1):13883, 2020.
- [31] Qunfeng Tang, Zhencheng Chen, Rabab Ward, Carlo Menon, and Mohamed Elgendi. Ppg2ecgps: An end-to-end subject-specific deep neural network model for electrocardiogram reconstruction from photoplethysmography signals without pulse arrival time adjustments. *Bioengineering*, 10(6):630, 2023.
- [32] Xiaoda Wang, Ching Chang, Defu Cao, Kaiqiao Han, Fang Sun, Yue Huang, Minxiao Wang, Chang Xu, Xiao Luo, Runze Yan, et al. Position: Beyond prediction: Toward verifiable physiological waveform reasoning with foundation models and agentic llms. In *The Forty-Third International Conference on Machine Learning*, 2026.

- [33] Jonas Wildberger, Maximilian Dax, Simon Buchholz, Stephen Green, Jakob H Macke, and Bernhard Schölkopf. Flow matching for scalable simulation-based inference. *Advances in Neural Information Processing Systems*, 36:16837–16864, 2023.
- [34] Ling Yang, Zhilong Zhang, Yang Song, Shenda Hong, Runsheng Xu, Yue Zhao, Wentao Zhang, Bin Cui, and Ming-Hsuan Yang. Diffusion models: A comprehensive survey of methods and applications. *ACM computing surveys*, 56(4):1–39, 2023.

## A Related Work

### A.1 Latent Generative Models

Diffusion and score-based generative models have become powerful tools for learning complex data distributions by gradually transforming noise into structured samples [12, 6, 34, 23, 18]. To improve computational efficiency, latent diffusion models move the generative process from the raw data space to a compressed latent space, reducing the cost of modeling high-dimensional signals while preserving sample quality [25]. This idea is particularly relevant for physiological waveform generation, where long temporal sequences can make direct generative modeling expensive and unstable [21]. Flow-based generative models provide an alternative continuous-time view of generation. Flow matching learns vector fields that transport simple base distributions to data distributions without simulating stochastic diffusion during training [19, 29, 33]. Rectified flow further encourages trajectories to follow straight transport paths between source and target distributions, enabling efficient sampling with coarse numerical integration [16, 9]. These properties make rectified flow attractive for PPG-to-ECG generation, where the model must transport PPG-conditioned latent variables toward plausible ECG representations. Existing latent flow methods for PPG-to-ECG generation have shown strong empirical performance [10], but their transport objectives are still largely statistical.

### A.2 Cross-Modal Physiological Representation Learning

Learning aligned representations across physiological modalities is central to translating PPG into ECG. Since PPG and ECG are generated by different but coupled physiological processes, successful cross-modal learning must balance modality-specific feature extraction with shared cardiovascular abstraction. Prior methods often encourage alignment by using shared encoders, contrastive objectives, or paired latent reconstruction. CardioPPG aligns PPG and ECG embeddings through cross-modal contrastive learning before using the aligned PPG encoder for downstream cardiovascular prediction and ECG synthesis [7]. PPGFlowECG similarly builds a shared latent space through a CardioAlign encoder and performs ECG generation in that aligned space [10]. These approaches demonstrate that latent alignment can improve downstream utility and generation quality.

## B The Electro-Hemodynamic Physiological Simulator

### B.1 Euler Discretization

We solve the electro-hemodynamic simulator with a fixed-step explicit Euler method. For any state variable  $u(t)$  satisfying  $du/dt = v(t)$ , the finite-difference approximation is

$$\frac{du}{dt}(t) \approx \frac{u(t + \Delta t) - u(t)}{\Delta t}, \quad (29)$$

which gives the Euler update

$$u(t + \Delta t) = u(t) + v(t)\Delta t. \quad (30)$$

For the coupled simulator state  $(x(t), y(t), e(t), p(t))$ , at time  $t_\ell = \ell\Delta t$ , the vector field is

$$\mathbf{v}_\ell = (f_x(x_\ell, y_\ell), f_y(x_\ell, y_\ell), f_e(x_\ell, y_\ell, e_\ell, t_\ell; \eta_e), f_p(x_\ell, y_\ell, p_\ell, t_\ell; \eta_p)). \quad (31)$$

The Euler updates are

$$x_{\ell+1} = x_\ell + f_x(x_\ell, y_\ell)\Delta t, \quad (32)$$

$$y_{\ell+1} = y_\ell + f_y(x_\ell, y_\ell)\Delta t, \quad (33)$$

$$e_{\ell+1} = e_\ell + f_e(x_\ell, y_\ell, e_\ell, t_\ell; \eta_e)\Delta t, \quad (34)$$

$$p_{\ell+1} = p_\ell + f_p(x_\ell, y_\ell, p_\ell, t_\ell; \eta_p)\Delta t. \quad (35)$$

### B.2 Fitting Objective

**Motivation.** The electro-hemodynamic simulator contains coupled electrical and hemodynamic components: the ECG readout represents upstream cardiac electrical activation, while the PPG readout represents the delayed and smoothed peripheral vascular response. Directly fitting this simulator

with a single point-wise waveform loss is often insufficient. A waveform loss may match the global amplitude envelope while missing sharp QRS transitions, systolic upstrokes, or physiologically meaningful event timing. We therefore optimize the simulator parameters with a composite objective that combines waveform-level reconstruction, derivative consistency, and event-level peak alignment. This design encourages the fitted parameters to reproduce both the electrical source dynamics and the downstream hemodynamic response.

Let  $e(t)$  and  $p(t)$  denote the reference ECG and PPG waveforms, and let  $\hat{e}_\eta(t)$  and  $\hat{p}_\eta(t)$  denote the simulated ECG and PPG waveforms generated by the electro-hemodynamic simulator with parameters  $\eta = (\eta_e, \eta_p)$ . The total fitting objective is

$$\mathcal{L}_{\text{fit}}(\eta) = \lambda_{\text{ecg}} \mathcal{L}_{\text{ecg}} + \lambda_{\text{ppg}} \mathcal{L}_{\text{ppg}} + \lambda_{\text{deriv}} \mathcal{L}_{\text{deriv}} + \lambda_{\text{peak}} \mathcal{L}_{\text{peak}}. \quad (36)$$

Unless otherwise specified, we use  $\lambda_{\text{ecg}} = 5.0$ ,  $\lambda_{\text{ppg}} = 0.25$ ,  $\lambda_{\text{deriv}} = 3.0$ , and  $\lambda_{\text{peak}} = 12.0$ .

**ECG waveform reconstruction.** The ECG reconstruction term anchors the simulator to the electrical component of the cardiac cycle:

$$\mathcal{L}_{\text{ecg}} = \frac{1}{T_e} \sum_{t=1}^{T_e} \|\hat{e}_\eta(t) - e(t)\|_2^2. \quad (37)$$

We assign this term a relatively large weight because the ECG is the primary physiological source that drives the downstream hemodynamic response. In practice, this term stabilizes the fitting of QRS-dominated electrical morphology and prevents the simulator from matching peripheral PPG morphology at the expense of unrealistic ECG dynamics.

**PPG waveform reconstruction.** The PPG reconstruction term measures the discrepancy between the simulated and reference peripheral pulse waveforms:

$$\mathcal{L}_{\text{ppg}} = \frac{1}{T_p} \sum_{t=1}^{T_p} \|\hat{p}_\eta(t) - p(t)\|_2^2. \quad (38)$$

Compared with ECG, PPG is an indirect observation affected by pulse transit time, vascular compliance, peripheral filtering, sensor contact, and amplitude variation. Therefore, we use a smaller weight for this term. This allows PPG to guide the hemodynamic readout without dominating the optimization or distorting the fitted electrical source.

**Derivative consistency.** To preserve local dynamic structure, we further match temporal derivatives:

$$\mathcal{L}_{\text{deriv}} = \frac{1}{T_e - 1} \sum_{t=1}^{T_e-1} \|\nabla \hat{e}_\eta(t) - \nabla e(t)\|_2^2 + \frac{1}{T_p - 1} \sum_{t=1}^{T_p-1} \|\nabla \hat{p}_\eta(t) - \nabla p(t)\|_2^2, \quad (39)$$

where  $\nabla x(t) = x(t+1) - x(t)$  denotes the first-order finite difference. This term emphasizes fast physiological transitions, such as steep QRS slopes in ECG and the systolic upstroke in PPG. It is also less sensitive to slow baseline drift and global amplitude offsets than pure waveform reconstruction. The derivative loss therefore encourages the simulator to reproduce local transition speed and morphology, rather than only matching low-frequency signal shape.

**Peak alignment.** Event timing is central to electro-hemodynamic coupling. We therefore include a peak alignment term that focuses on local neighborhoods around detected physiological events, such as ECG R-peaks and PPG systolic peaks. Let  $\mathcal{R}$  denote the set of detected ECG R-peak indices and  $\mathcal{S}$  denote the set of detected PPG systolic peak indices. For an event index  $\tau$ , let  $\Omega(\tau)$  denote a local temporal window around the event. In our implementation, the window is defined by 0.20 seconds before and 0.60 seconds after the event. The peak alignment loss is

$$\mathcal{L}_{\text{peak}} = \frac{1}{|\mathcal{R}|} \sum_{\tau \in \mathcal{R}} \frac{1}{|\Omega_e(\tau)|} \sum_{t \in \Omega_e(\tau)} \|\hat{e}_\eta(t) - e(t)\|_2^2 + \frac{1}{|\mathcal{S}|} \sum_{\tau \in \mathcal{S}} \frac{1}{|\Omega_p(\tau)|} \sum_{t \in \Omega_p(\tau)} \|\hat{p}_\eta(t) - p(t)\|_2^2. \quad (40)$$

This term receives the largest weight because peak locations define key physiological timing events. Matching peaks only through global waveform losses can be unstable: a small temporal shift may cause a large point-wise error even when the morphology is otherwise similar. By explicitly emphasizing local event neighborhoods, the peak loss encourages beat-level synchronization and improves the fitted pulse-arrival relationship between ECG and PPG.

**Staged electro-hemodynamic optimization.** We use a simple curriculum to stabilize fitting. During the initial portion of training, controlled by  $\rho_{\text{ecg}} = 0.5$ , we optimize only ECG-related terms:

$$\mathcal{L}_{\text{warmup}}(\eta) = \lambda_{\text{ecg}}\mathcal{L}_{\text{ecg}} + \lambda_{\text{deriv}}\mathcal{L}_{\text{deriv}}^e + \lambda_{\text{peak}}\mathcal{L}_{\text{peak}}^e, \quad (41)$$

where  $\mathcal{L}_{\text{deriv}}^e$  and  $\mathcal{L}_{\text{peak}}^e$  denote the ECG components of the derivative and peak losses. After this warm-up stage, we optimize the full electro-hemodynamic objective in Eq. 36. This staged design first stabilizes the cardiac electrical source and then introduces the more indirect PPG constraints. It reduces poor local minima in which the simulator prematurely fits delayed peripheral pulse morphology while the underlying ECG dynamics remain inaccurate.

The composite fitting objective assigns different roles to complementary physiological constraints. The ECG waveform loss stabilizes the electrical source, the PPG waveform loss guides the delayed vascular response, the derivative loss preserves fast local dynamics, and the peak alignment loss enforces event-level timing. Together, these terms produce simulator parameters that better capture both ECG morphology and ECG-to-PPG hemodynamic coupling, which are later used as physiological anchors for simulator-guided latent flow training.

**ICD-stratified simulator fitting.** We use the top-100 most frequent ICD-10 codes in the training split to define simulator fitting groups. For each group, representative ECG-PPG beat crops are collected from training samples and used to fit the simulator parameters with the objective in Eq. (??). The fitted parameters are fixed afterward and used only for simulator residual losses during flow training. ICD labels are never used as inputs to the generator and are not required during inference.

### B.3 Consistency interpretation of Euler residual losses.

The fitted electro-hemodynamic parameters are used to define simulator vector-field residuals on terminal generated beats during latent-flow training. We provide a simple consistency interpretation showing that minimizing these residuals keeps the generated beat close to a trajectory induced by the physiological simulator. For modality  $m \in \{e, p\}$ , let  $\tilde{h}^m = (\tilde{h}_1^m, \dots, \tilde{h}_{L_m}^m)$  denote a generated beat crop, where  $m = e$  corresponds to ECG and  $m = p$  corresponds to PPG. Let  $f_m$  be the corresponding simulator vector field with fitted parameters  $\eta_m$ , and let  $s_\ell^m = (x_\ell^m, y_\ell^m)$  denote the reference cardiac phase state at step  $\ell$ . The Euler residual is

$$r_\ell^m = \frac{\tilde{h}_{\ell+1}^m - \tilde{h}_\ell^m}{\Delta t_m} - f_m(s_\ell^m, \tilde{h}_\ell^m, t_\ell^m; \eta_m). \quad (42)$$

Assume that  $f_m$  is  $K_m$ -Lipschitz in the waveform state and that the generated beat has bounded average Euler residual,

$$\frac{1}{L_m - 1} \sum_{\ell=1}^{L_m-1} \|r_\ell^m\|_2^2 \leq \epsilon_m^2. \quad (43)$$

Let  $h^{m,*}$  be the simulator trajectory initialized at the same first sample,

$$h_1^{m,*} = \tilde{h}_1^m, \quad h_{\ell+1}^{m,*} = h_\ell^{m,*} + \Delta t_m f_m(s_\ell^m, h_\ell^{m,*}, t_\ell^m; \eta_m). \quad (44)$$

Then the deviation between the generated beat and the simulator-induced trajectory satisfies

$$\max_{\ell \leq L_m} \|\tilde{h}_\ell^m - h_\ell^{m,*}\|_2 \leq \Delta t_m \exp(K_m T_m) \sum_{\ell=1}^{L_m-1} \|r_\ell^m\|_2, \quad (45)$$

where  $T_m = (L_m - 1)\Delta t_m$  is the beat duration. Equivalently, using Eq. 43,

$$\max_{\ell \leq L_m} \|\tilde{h}_\ell^m - h_\ell^{m,*}\|_2 \leq T_m \exp(K_m T_m) \epsilon_m. \quad (46)$$

**Proof sketch.** Let  $\delta_\ell = \|\tilde{h}_\ell^m - h_\ell^{m,*}\|_2$ . By the Euler update and the definition of  $r_\ell^m$ ,

$$\delta_{\ell+1} \leq \delta_\ell + \Delta t_m \left\| f_m(s_\ell^m, \tilde{h}_\ell^m, t_\ell^m; \eta_m) - f_m(s_\ell^m, h_\ell^{m,*}, t_\ell^m; \eta_m) \right\|_2 + \Delta t_m \|r_\ell^m\|_2. \quad (47)$$

Using the Lipschitz condition gives

$$\delta_{\ell+1} \leq (1 + K_m \Delta t_m) \delta_\ell + \Delta t_m \|r_\ell^m\|_2. \quad (48)$$

Since  $\delta_1 = 0$ , applying the discrete Gronwall inequality yields Eq. 45.

This result shows that the simulator-guided Euler residual losses do more than penalize point-wise waveform error. Under mild smoothness assumptions, small residuals imply that the generated ECG or PPG beat remains close to a trajectory generated by the fitted physiological vector field. Therefore, the ECG-side and PPG-side simulator losses constrain generated samples toward electro-hemodynamically plausible dynamics.

## C Why Physiology-Guided Latent Rectified Flow?

This section provides a concise theoretical justification for employing latent rectified flow within the PG-LRF framework. Rather than asserting that rectified flow is universally superior to alternative generative models, our objective is to clarify why it serves as a principled and stable mechanism for PPG-conditioned ECG generation when operating within a structured physiological latent space.

Let  $z_p = E_\phi^p(x_p)$  denote the PPG condition latent and  $z_e = E_\phi^e(x_e)$  denote the paired ECG latent. Following the optimization of the Physiology-Aware AutoEncoder (PAE), PG-LRF learns a conditional vector field that transports a Gaussian source latent  $z_0 \sim \mathcal{N}(0, I)$  toward the ECG latent distribution, conditioned on  $z_p$ . For a time variable  $t \sim \mathcal{U}(0, 1)$ , the linear interpolation path is defined as

$$z_t = (1 - t)z_0 + tz_e,$$

with the target velocity  $u_t = z_e - z_0$ . The latent rectified-flow objective is then formulated as

$$\mathcal{L}_{\text{RF}} = \mathbb{E} \left[ \|v_\psi(z_t, t, z_p) - (z_e - z_0)\|_2^2 \right].$$

**Conditional transport interpretation.** Given a fixed condition  $z_p$ , the population minimizer of  $\mathcal{L}_{\text{RF}}$  is

$$v^*(z, t, z_p) = \mathbb{E} [z_e - z_0 \mid z_t = z, t, z_p].$$

This follows from the standard result that the conditional mean minimizes the squared-error regression objective. Let  $p_t(z \mid z_p)$  denote the marginal distribution of  $z_t$  conditioned on  $z_p$ . For any smooth test function  $\varphi$ , differentiating along the interpolation path yields

$$\frac{d}{dt} \mathbb{E} [\varphi(z_t) \mid z_p] = \mathbb{E} [\nabla_z \varphi(z_t)^\top (z_e - z_0) \mid z_p].$$

Substituting the optimal vector field  $v^*$  results in

$$\frac{d}{dt} \mathbb{E} [\varphi(z_t) \mid z_p] = \mathbb{E} [\nabla_z \varphi(z_t)^\top v^*(z_t, t, z_p) \mid z_p],$$

which corresponds to the weak form of the continuity equation:

$$\partial_t p_t(z \mid z_p) + \nabla_z \cdot (p_t(z \mid z_p) v^*(z, t, z_p)) = 0.$$

Consequently, under standard regularity assumptions on the vector field, simulating the ordinary differential equation (ODE)  $\frac{dz_t}{dt} = v^*(z_t, t, z_p)$  deterministically transports the Gaussian source distribution to the conditional ECG latent distribution associated with the observed PPG latent  $z_p$ .

**Latent-space stability.** The above derivation formally justifies the generative process in the latent space. To connect this latent transport to target waveform generation, we assume the frozen ECG decoder  $D_\theta^e$  is  $L_D$ -Lipschitz continuous:

$$\|D_\theta^e(z_1) - D_\theta^e(z_2)\|_2 \leq L_D \|z_1 - z_2\|_2.$$

Let  $\hat{z}_e$  be the terminal latent produced by the learned flow and let  $\hat{x}_e = D_\theta^e(\hat{z}_e)$ . The waveform generation error can be bounded as

$$\|\hat{x}_e - x_e\|_2 \leq L_D \|\hat{z}_e - z_e\|_2 + \|D_\theta^e(z_e) - x_e\|_2.$$

This inequality demonstrates that the overall waveform error is strictly controlled by two components: the latent transport error (the flow model) and the reconstruction error (the frozen autoencoder). This theoretically justifies our two-stage methodology: ensuring that the PAE learns a faithful representation minimizes the reconstruction penalty  $\|D_\theta^e(z_e) - x_e\|_2$ , thereby allowing the rectified flow to focus entirely on optimizing the conditional transport.

**Role of physiological guidance.** The simulator-guided objective further regularizes this conditional transport:

$$\mathcal{L}_{\text{Flow}} = \mathcal{L}_{\text{RF}} + \lambda_e \mathcal{L}_{\text{sim}}^e + \lambda_p \mathcal{L}_{\text{sim}}^p.$$

In this formulation,  $\mathcal{L}_{\text{RF}}$  governs the statistical transport from the Gaussian prior to the empirical ECG latent distribution. Concurrently, the terms  $\mathcal{L}_{\text{sim}}^e$  and  $\mathcal{L}_{\text{sim}}^p$  bias the predicted terminal state toward trajectories that exhibit valid ECG morphology and forward ECG-to-PPG hemodynamic compatibility. Crucially, because these simulator constraints are applied exclusively during training via gradient signals along the flow trajectory, they do not strictly bound inference to a rigid simulator template. Instead, they function as soft physiological priors, narrowing the set of plausible solutions in the highly underdetermined PPG-to-ECG inverse problem.

In summary, PG-LRF operates as a regularized conditional transport framework: the PAE constructs a dense, physiology-aware manifold, the rectified flow learns an optimal deterministic transport upon it, and the simulator guidance anchors the generated distributions to electro-hemodynamically plausible dynamics.

## D Implementation details.

PG-LRF is trained in PyTorch on NVIDIA H200 in two stages. In the first stage, we train the Physiology-Aware AutoEncoder (PAE) to map native-rate PPG and ECG segments into a shared electro-hemodynamic latent space. The input PPG segment has length 400 at 40 Hz, and the input ECG segment has length 1200 at 120 Hz. Both modalities are normalized with per-sample z-score normalization. The PAE encoder first processes PPG and ECG with modality-specific stems, then passes the representations through shared blocks with lightweight modality-aware adapters, and finally maps them to a common Gaussian latent posterior. The decoder reconstructs waveforms at their native temporal resolutions using a residual reconstruction branch and a lightweight decomposition branch that models level, trend, and seasonal components. The PAE is optimized with AdamW using a learning rate of  $2 \times 10^{-5}$  and batch size 4 for 120K iterations. The KL weight is set to  $5 \times 10^{-5}$  with a 5K-iteration linear warmup. To encourage cross-modal latent alignment, we use global posterior alignment with weight  $5 \times 10^{-5}$  and 10K-iteration warmup, cross-modal semantic decodability with weight  $5 \times 10^{-4}$ , and bidirectional InfoNCE instance discrimination with weight  $10^{-3}$ .

In the second stage, we freeze the PAE encoder and decoder and train only the PPG-conditioned latent rectified flow. The target is the ECG latent encoded from the paired ECG segment, while the condition is the PPG latent encoded from the synchronized PPG segment. The rectified-flow model uses a Transformer backbone with latent channel size 4, temporal length 50, depth 4, hidden dimension 256, and 4 attention heads. During training, Gaussian noise is linearly interpolated with the target ECG latent, and the model learns the conditional vector field from multiple random time points. We sample 4 time points per forward pass and optimize the mean-squared rectified-flow objective. The latent rectified flow is trained with Adam using a base learning rate of  $1 \times 10^{-4}$  and betas (0.9, 0.96) for 50K iterations. We use warmup and ReduceLROnPlateau scheduling, with 1K warmup steps, patience 1K, and decay factor 0.5. Gradients are clipped to a maximum norm of 1.0. An exponential moving average model is maintained with decay 0.995 and updated every 10 steps. Checkpoints are saved every 1K iterations. Both stages are trained on a single GPU with batch size 4, shuffled data loading, pinned memory, and 16 CPU workers.

And  $\Theta_e(\cdot)$  and  $\Theta_p(\cdot)$  are implemented as differentiable soft phase estimators based on local peak-response maps, allowing gradients to propagate through the reconstructed waveforms.

## E Limitations

This work has several limitations. Our experiments are conducted on MC-MED, a real-world emergency-department monitoring dataset. Although it provides synchronized ECG and PPG recordings, evaluation on additional datasets is needed to further assess generalization.